AlGaSb/GaSb quantum wells grown on an optimized AlSb nucleation layer*

Gao Hanchao(高汉超), Wen Cai(温才), Wang Wenxin(王文新)†, Jiang Zhongwei(蒋中伟), Tian Haitao(田海涛), He Tao(何涛), Li Hui(李辉), and Chen Hong (陈弘)

(Beijing National Laboratory for Condensed Matter Physics, Institute of Physics, Chinese Academy of Sciences, Beijing 100190, China)

Abstract: Five-period AlGaSb/GaSb multiple quantum wells (MQW) are grown on a GaSb buffer. Through optimizing the AlSb nucleation layer, the low threading dislocation density of the MQW is found to be $(2.50 \pm 0.91) \times 10^8$ cm^{-2} in 1-μm GaSb buffer, as determined by plan-view transmission election microscopy (TEM) images. High resolution TEM clearly shows the presence of 90° misfit dislocations with an average spacing of 5.4 nm at the AlSb/GaAs interface, which effectively relieve most of the strain energy. In the temperature range from $T = 26$ K to 300 K, photoluminescence of the MQW is dominated by the ground state electron to ground state heavy hole (e1–hh1) transition, while a high energy shoulder clearly seen at $T > 76$ K can be attributed to the ground state electron to ground state light hole (e1–lh1) transition.

Key words: molecular beam epitaxy; antimonide; semiconducting III–V material
DOI: 10.1088/1674-4926/31/5/053003 **PACC:** 8115; 7280E; 7865J

1. Introduction

For the past decades there has been growing interest in the application of antimonide-based III–V compound semiconductors for infrared, optical and high-speed devices[1−4]. So far, heteroepitaxy on GaAs (001) substrate has most commonly been used to grow these semiconductors. Due to the large lattice mismatch between the GaSb epilayer and the GaAs substrate ($\Delta a/a = 7.8\%$), the epilayer has high density threading dislocations. To make the GaSb buffer smoother, AlSb as a nucleation layer is always used in GaSb/GaAs epitaxy[5]. It is known that the dislocation density of the GaSb buffer depends on the growth conditions of the AlSb nucleation, such as thickness, temperature and V/III ratio (the V and III group element atoms which reach the substrate surface ratio, namely, the beam equilibrium pressure ratio)[6]. However, in the literature there are few reports on the optimization of AlSb growth on GaAs substrate. In this work, we report growth of AlGaSb/GaSb multiple quantum wells (MQW) with optimized growth temperature and rate for the AlSb nucleation layer.

2. Experiments

GaSb layers were grown on a (001) GaAs substrate in a VG V80H MBE system with a conventional effusion antimony cell. The Sb_4 was used to grow GaSb and AlSb. Prior to the growth, surface oxide was desorbed from the GaAs surface under As_2-rich flux protection at 580 °C measured with a thermocouple calibrated by an IRCON infrared pyrometer. According to our experimental experience and Ref. [6], a 9-nm AlSb nucleation layer, which has been proven decrease dislocation effectively[6], was first deposited on a smooth GaAs buffer, then a 500-nm GaSb buffer was grown on the AlSb nucleation layer. Different AlSb growth temperatures and growth rates were selected to optimize the growth condition of the AlSb nucleation layer. The V/III ratio was fixed at 10 for AlSb and GaSb deposition. The detailed growth parameters of AlSb nucleation and the FWHM of GaSb (004) ω scan results are shown in Table 1. The crystalline quality of the GaSb buffer was characterized by high resolution X-ray diffraction (HRXRD) and high resolution TEM (HRTEM). Therefore, the optimized growth conditions for the AlSb nucleation layer were found. Then AlGaSb/GaSb MQW have been grown on GaAs substrates with a GaSb buffer grown at optimized AlSb nucleation conditions. Photoluminescence (PL) was used to determine the optical properties of the MQW structures.

The crystalline quality was characterized by HRXRD (a BEDE D 1 system, with CuK$\alpha = 1.5432$) and HRTEM (a JEOL 2010 HRTEM system, with $C_s = 0.5$ mm point resolution of 0.194 nm). The surface roughness is determined by AFM. PL spectra were measured at temperatures from 26 K to 300 K using a 632.8 nm He–Ne laser, with a 50 cm monochrometer and InGaAs detector.

3. Results and discussion

3.1. HRXRD and HRTEM

Rocking curve ω-scans and the surface morphology of the GaSb buffer have been determined by HRXRD. The full width at half maximum (FWHM) of GaSb (004) ω-scans is shown in Fig. 1(a), against the growth temperature of the AlSb layer from $T = 360$ to 530 °C. As can be seen, the samples have the smallest FWHM and hence the best crystalline quality when the AlSb nucleation layer is grown during 490–520 °C.

Figure 1(b) shows the dependence of the FWHM on the growth rate of the AlSb nucleation layer, at a fixed growth tem-

* Project supported by the National Natural Science Foundation of China (No. 50572120), the National High Technology Research and Development Program of China (No. 2009AA033101), and the State Key Development for Basic Research of China (No. 2010CB327501).
† Corresponding author. Email: wxwang@aphy.iphy.ac.cn
Received 23 April 2009, revised manuscript received 12 January 2010

Table 1. Basic growth parameters of the AlSb nucleation layer and corresponding FWHM of GaSb(004) ω-scans.

Sample	V/III ratio	Growth temperature (°C)	Thickness (nm)	Growth rate (ML/s)	FWHM (arcsec)
1	10	530	9	0.453	660
2	10	520	9	0.453	463
3	10	490	9	0.453	449
4	10	450	9	0.453	481
5	10	420	9	0.453	468
6	10	360	9	0.453	517
7	10	490	9	0.136	389
8	10	490	9	0.272	344
9	10	490	9	0.453	424

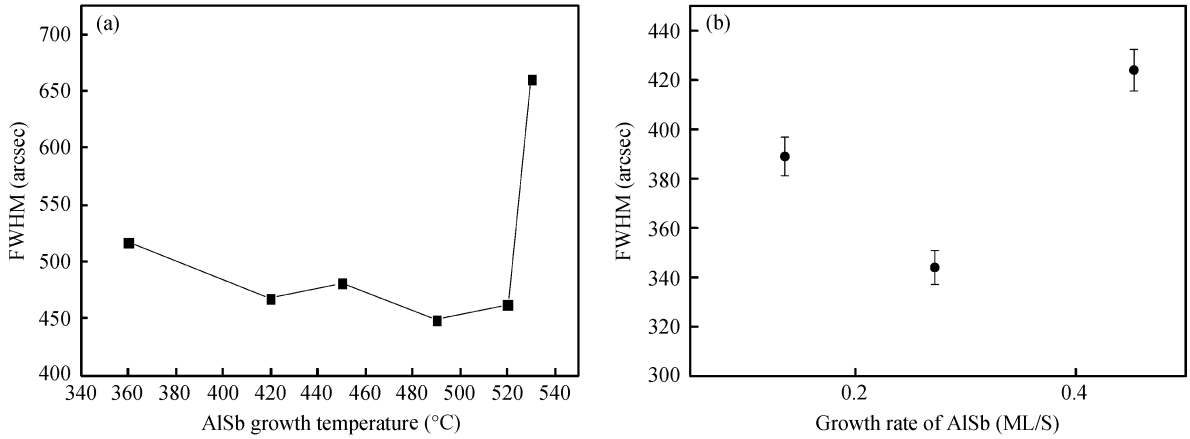

Fig. 1. (a) FWHM and root mean square (RMS) surface roughness of the GaSb layer versus the growth temperature of AlSb. The thickness is 9 nm and the growth rate is 0.453 ML/s. Solid circles and solid squares represent the FWHM and RMS respectively. (b) FWHM of HRXRD of the GaSb buffer with different AlSb growth rates at a fixed temperature of 490 °C The thickness is 9 nm and the V/III ratio is 10.

perature $T = 490\,^{\circ}\mathrm{C}$. At $T = 490\,^{\circ}\mathrm{C}$ the sample has the best crystalline quality with a growth rate of 0.272 ML/s. The dependence of crystalline quality on AlSb growth rate may come from the surface diffusion of Al atoms[7]. Therefore, we have found a set of optimized AlSb nucleation conditions: AlSb thickness is 9 nm, V/III ratio is 10 and growth rate is 0.273 ML/s. After optimization of the AlSb nucleation conditions, five periods of AlGaSb/GaSb QWs are then grown on GaAs substrates using a 1 μm GaSb buffer on the AlSb nucleation layer. The structure of the QW is 30 nm AlGaSb / 5 nm GaSb / 30 nm AlGaSb.

It is well known that HRXRD is a powerful tool to study the crystalline quality, and the triple-axis crystal ω scan is an effective way to investigate the mosaicity of the epitaxial layer directly and the dislocation densities indirectly[8, 9]. The dislocation density related FWHM of XRD can be expressed as follows[18]: $N_{\mathrm{s}} = a_{\omega}^2/4.36b^2$, where N_{s} is the dislocation density, a_{ω} is the FWHM of the ω scan and b is the Burgers vector. Figure 2 shows the triple-axis crystal rocking curve of the GaSb buffer of a MQW. The FWHM of this buffer is very narrow ($a_{\omega} < 200$ arcsec), corresponding to a dislocation density of 9.1×10^7 cm^{-2}. To determine the actual value of the threading dislocation density, plan-view TEM images have been used. Figure 3(a) shows a plan-view TEM image. Different regions of the sample have been selected extensively to determine the density of the threading dislocation. The obtained density of threading dislocation is about $(2.50 \pm 0.91) \times 10^8$ cm^{-2}, which is not far from the value estimated from XRD.

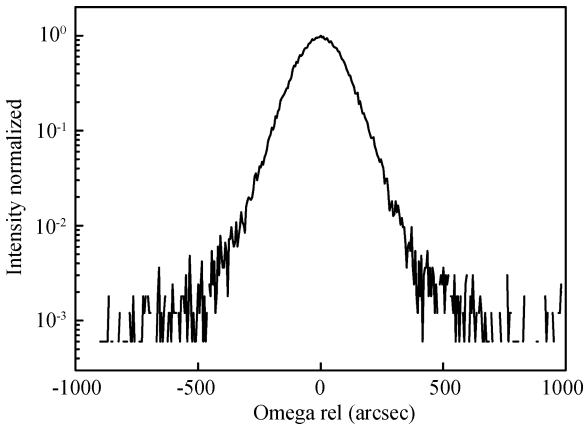

Fig. 2. Triple-axis crystal rocking curve of the GaSb(004) buffer of MQW sample.

Figure 3(b) shows the cross-sectional HRTEM image of the MQW structure. Though some vertical propagating defects originating from the interface can be observed in the GaSb buffer, the MQW region can be clearly seen and there is no obvious threading dislocation. Therefore, the threading dislocations have been effectively minimized by the AlSb nucleation layer and GaSb buffer layer.

Figure 4 shows the HRTEM image of the AlSb/GaAs interface and the inset is the corresponding SAED pattern. Because the substrate is thick enough, the deformation of the sub-

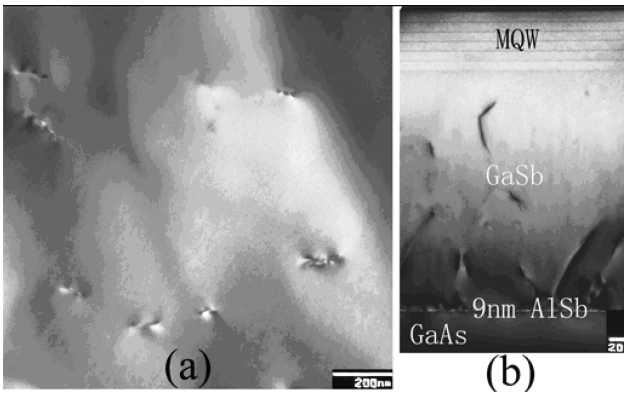

Fig. 3. TEM image of AlGaSb/GaSb quantum well. (a) Plan-view TEM image. (b) Cross-sectional TEM image.

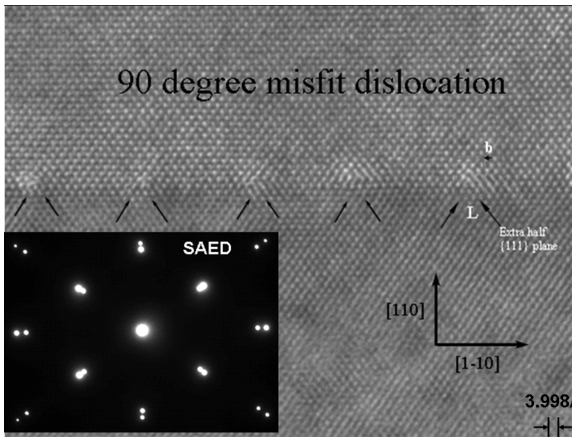

Fig. 4. HR-TEM image taken from the AlSb/GaAs (001) interface. The Burgers vector $\boldsymbol{b}$ of the dislocation labeled L was determined to be $\frac{1}{2}\langle 110\rangle$ by applying the Burgers circuit by the right-hand/finish-start (RH/FS) convention[19]. Furthermore, according to the structural characteristics of the dislocations in zinc-blende structure crystal, it was determined to be a 90° dislocation[20]. Extra {111} planes of each dislocation are marked by arrows. The inset picture is the corresponding selected area electron diffraction (SAED) pattern of the AlSb/GaAs interface.

strate can be assumed to be negligible. Thus GaAs can be used as a reference for determining the actual lattice parameter of the film. The image clearly shows the presence of a 90° misfit dislocation array at the AlSb/GaAs interface, which releases most of the strain energy. The average spacing between the 90° misfit dislocations is approximately 5.4 nm. The spacing S of the misfit dislocation array depends on the misfit δ. The S can be determined by the formula $S = d/\delta$. d is the $AlSb_{110}$ spacing distance, and $\delta = 0.0853$ is the misfit between AlSb and GaAs. If the system has the 90° misfit dislocation array structure, the S is 5.08 nm which is much smaller than the experimental value. The $AlSb_{110}$ lattice parameter measured by SAED is about 0.43 ± 0.001 nm which is smaller than the $AlSb_{110}$ bulk lattice parameter 0.4338 nm. This indicates that the lattice of AlSb film has small deformation, which can influence the average spacing of misfit dislocation. Considering the deformation only, misfit δ and the spacing S can be calculated as $\delta = (d_{\mathrm{AlSb110}} - d_{\mathrm{GaAs110}})/d_{\mathrm{GaAs110}} = 0.076$ and

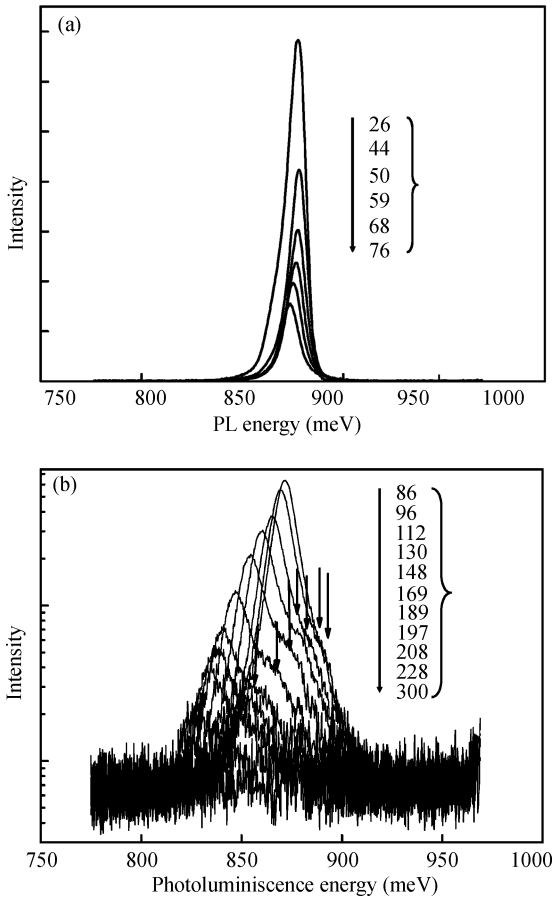

Fig. 5. (a) PL spectra obtained at temperatures from 26 K to 76 K. The spectra have only one peak corresponding to the e1-hh1 transition. (b) In the temperature range from 86 K to 246 K, another peak corresponding to the e1–lh1 transition was observed, as marked by arrows.

$S = d_{\mathrm{AlSb110}}/0.076 = 5.66$ nm which is larger than 5.40 nm. However, the interfacial plane curve also plays a role in spacing. When the strain is compressive, the island tends to expand along the interface but is constrained by the substrate. The surface bending phenomenon makes the misfit dislocation spacing small[17]. Therefore, the average spacing $S = 5.4$ nm is a combination of the effects of lattice deformation and the surface bending phenomenon.

3.2. Photoluminescence

PL has been used to determine the optical properties of the MQW from 26 K to 300 K. As shown in Fig. 5(a), only one peak corresponding to the e1–hh1 transition is observed around 875 meV, in the PL spectra from $T = 26$ K to 76 K. Nevertheless, as shown in Fig. 5(b), another peak is observed at the high energy tail from $T = 86$ K to 300 K. For example, the peak position of the photoluminescence transition (e1–hh1) at 96 K is 866 meV, and at the high energy tail, a shoulder gives rise to a peak at about 884 meV, presumably corresponding to the transition from ground state electron to ground state light hole (e1–lh1).

We have used a one-dimension finite quantum well model to calculate the energy bands of the MQW, the parameters used for $T = 96$ K are shown in Fig. 6. The calculation gives an

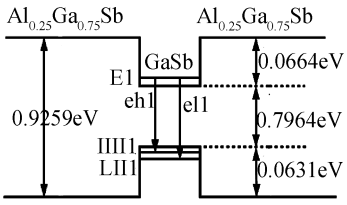

GaSb	$Al_{0.25}Ga_{0.75}Sb$
m_e=0.039	m_e=0.0693
m_{hh}=0.25	m_{hh}=0.3875
m_{lh}=0.04	m_{lh}=0.063

Fig. 6. The one-dimension finite well model and the corresponding parameters for calculation. The parameters used in the model are from Ref. [10–12].

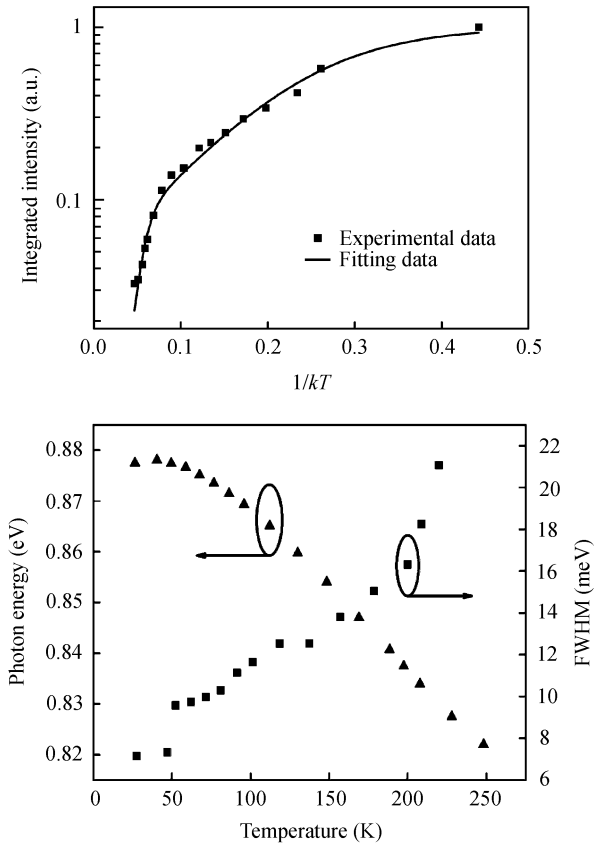

Fig. 7. (a) PL intensity versus $1/kT$. The solid line is the fitting curve using Eq. (1). (b) Temperature dependence of the PL peak energy and FWHM for the MQW.

e1–lh1 transition energy of 883.8 meV at $T = 96$ K, which agrees very well with the experimental data. The temperature dependence of the observability of the e1-lh1 emission may be attributed to thermal activation. There are not enough light holes to recombine with electrons below 76 K, so the peak e1-lh1 cannot be observed. When the temperature increases to 86 K, thermal activation generates enough light holes and radiative recombination happens.

Figure 7(a) shows the integrated PL intensities of the sample plotted against inverse temperature from 26 K to 300 K. The sample shows two remarkable temperatures regimes which obey Arrhenius dependence. This behavior corresponds to two thermally activated nonradiative recombination mechanisms where the slopes of the straight line portions of the curves give the activation energies for the two processes. The temperature dependence of PL intensity would be of the form

$$I = I_0\left[1 + C_1 \exp\left(-\frac{E_a}{k_b T}\right) + C_2 \exp\left(-\frac{E_b}{k_b T}\right)\right], \quad (1)$$

where k_b is Boltzmann's constant, C_1, C_2, and I_0 are constants independent of temperature. The experimental data were fitted using Eq. (1), and the activation energies are $E_a = 13$ meV, $E_b = 129$ meV. The activation E_a is most likely caused by nonradiative traps, perhaps due to a deep acceptor, neutral impurity or vacancy related defects. The short PL lifetimes that have been measured at room temperature also indicate that the high-temperature luminescence is dominated by nonradiative recombination[13, 14]. The MQW sample has lots of dislocations that can be observed in plan-view TEM images. Dislocations can generate nonradiative centers. The sample has bad luminescence signals at high temperature, meaning that the large E_a is probably caused by dislocations and other nonradiative recombination.

Figure 7(b) shows the temperature dependence of the photon energy and FWHM. The relationship between the FWHM and the temperature can be influenced by several factors, such as phonon scattering and ionized impurity scattering. With increasing temperature, FWHM always grows linearly or sublinearly[15, 16]. In our case, the temperature dependence of FWHM also exhibits sublinear behavior. The photon energy of photoluminescence decreases with increasing temperature. The photon energy and FWHM measured at 26 K were 877 and 7.15 meV, respectively. The corresponding wavelength is 1413 nm between 1300 nm and 1550 nm which can be used for optical fiber communication.

4. Conclusions

AlGaSb/GaSb QWs have been successfully grown on GaAs substrate by optimizing the AlSb growth process. AlSb as an effective nucleation layer can effectively minimize the threading defect and relieve strain energy. An optimized AlSb nucleation layer can reduce the threading dislocation density to $(2.50 \pm 0.91) \times 10^8$ cm^{-2}. The strain energy is relieved by 90° misfit dislocation at the AlSb/GaAs interface. Due to a combination of the effects of lattice deformation and the surface curve, the average spacing of the misfit array is larger than the theoretical data. The photoluminescence of the MQWs exhibits an e1–lh1 transition above 76 K, which can be explained by a one-dimension model. The emission wavelength around 1.4 μm is observed at 26 K.

References

[1] Samoska L, Brar B, Kroemer H. Strong far-infrared intersubband absorption under normal incidence in heavily n-type doped nonalloy GaSb-AlSb superlattices. Appl Phys Lett, 1993, 62: 2539

[2] Zhang Y, Baruch N, Wang W I. Normal incidence infrared photodetectors using intersubband transitions in GaSb L-valley quantum wells. Appl Phys Lett, 1993, 63: 1068

[3] Shterengas L, Belenky G, Kipshidze G, et al. Room temperature operated 3.1 μm type-I GaSb-based diode lasers with 80 mW continuous-wave output power. Appl Phys Lett, 2008, 92: 171111

[4] Bolognesi C R, Caine E J, Kroemer H. Improved charge control and frequency performance in InAs/AlSb-based heterostructure

field-effect transistors. IEEE Electron Device Lett, 1994, EDL-15: 16

[5] Kroemer H. The 6.1 Å family (InAs, GaSb, AlSb) and its heterostructures: a selective review. Physica E. 2004, 20: 196

[6] Kim H S, Noha Y K, Kim M D, et al. Dependence of the AlSb buffers on GaSb/GaAs(001) heterostructures. J Cryst Growth, 2007, 301/302: 230

[7] Hao Ruiting, Xu Yingqiang, Zhou Zhiqiang, et al. Growth of GaSb layers on GaAs (001) substrate by molecular beam epitaxy. J Phys D: Appl Phys, 2007, 40: 1080

[8] Yuan K, Radhakrishnan K, Zheng H Q, et al. Characterization of linearly graded metamorphic InGaP buffer layers on GaAs using high-resolution X-ray diffraction. Thin Solid Films, 2001, 391: 36

[9] Heying B, Wu X H, Keller S, et al. Role of threading dislocation structure on the X-ray diffraction peak widths in epitaxial GaN films. Appl Phys Lett, 1996, 68: 643

[10] Leroux M, Massies J. Monolayer control in the growth of (Al,Ga)Sb/GaSb single quantum wells: application to the band offset and Γ–L crossover problems. Appl Phys Lett, 1996, 68: 54

[11] Mathieu H, Auvergne D, Merle P, et al. Electronic energy levels in $Ga_{1-x}Al_xSb$ alloys. Phys Rev B, 1975,12 : 5846

[12] Vurgaftmana I, Meyer J R, Ram-Mohan L R. Band parameters for III–V compound semiconductors and their alloys. J Appl Phys, 2001, 89: 5815

[13] Toyota H, Sasaki T, Jinbo Y, et al. Growth and characterization of GaSb/AlGaSb multi-quantum well structures on Si (001) substrates. J Cryst Growth, 2008, 310: 78

[14] Lambkin J D, Considine L, Walsh S, et al. Temperature dependence of the photoluminescence intensity of ordered and disordered $In_{0.48}Ga_{0.52}P$. Appl Phys Lett, 1994, 65: 73

[15] Veliadis J V D, Khurgin J B, Ding Y J, et al. Investigation of the photoluminescence-linewidth broadening in periodic multiple narrow asymmetric coupled quantum wells. Phys Rev B, 1994, 50: 4463

[16] Lee J, Koteles E S, Vassell M O. Luminescence linewidths of excitons in GaAs quantum wells below 150 K. Phys Rev B, 1986, 33: 5512

[17] Kim Y H, Lee J Y, Noh Y G, et al. High-resolution transmission electron microscopy study on the growth modes of GaSb islands grown on a semi-insulating GaAs (001) substrate. Appl Phys Lett, 2007, 90: 241915

[18] Ayers J E. The measurement of threading dislocation densities in semiconductor crystals by X-ray diffraction. J Cryst Growth, 1994, 135: 71

[19] Hull D, Bacon D J. Introduction to dislocations. Oxford: Butterworth-Heinemann, 2001: 17

[20] Lazar M, Wagner G. Calculation of displacement fields and simulation of HRTEM images of dislocations in sphalerite type A(III)B(V) compound semiconductors. Cryst Res Technol, 1997, 32: 111